Structure and lithium ionic conduction in W-doped Li$_{0.39}$La$_{0.54}$TiO$_3$ perovskite solid electrolyte

YAZHOU KONG[a,b], YING LI[a,*]

[a]*School of Metallurgy, Northeastern University, Shenyang 110819, China*
[b]*National & Local Joint Engineering Research Center for Mineral Salt Deep Utilization, Faculty of Chemical Engineering, Huaiyin Institute of Technology, Huaian 223003, China*

In this work, effect of W doping on crystalline structure, microstructure and conductivity for Li$_{0.39}$La$_{0.54}$TiO$_3$ perovskite-type solid electrolyte were investigated. Influence of protection method during sintering on crystalline structure for W-doped Li$_{0.39}$La$_{0.54}$TiO$_3$ was also studied. X-ray diffraction, scanning electron microscope and AC-impedance spectra technology were used to characterize solid electrolyte samples. (Li$_{0.39}$La$_{0.54}$)$_{(1-x)}$Ti$_{(1-x)}$W$_x$O$_3$ (x=0, 0.01, 0.03, 0.06) present perovskite structure. With the increase of W dopant content, conductivity of solid electrolyte first increases then decreases. Among all compounds, Li$_{0.36}$La$_{0.51}$Ti$_{0.97}$W$_{0.03}$O$_3$ has the highest total conductivity of 5.94×10^{-5} S cm^{-1} at room temperature with activation energy of 0.314 eV.

1. Introduction

All solid state lithium-based batteries are considered to be next generation of energy storage devices for electrical vehicles and electronic devices [1, 2, 3]. All solid state lithium batteries have high energy density and excellent safety performance [3]. Inorganic Li ion conductor are promising solid electrolyte for All solid state Lithium-based batteries [4]. Li ion conducting inorganic materials such as LiPON, Li-Ge-P-S, Li-La-Zr-O and Li$_{3x}$La$_{2/3-x}$TiO$_3$ (LLTO) have been reported as solid electrolyte due to high ionic conductivity. [5] Among these inorganic solid electrolytes, perovskite-type Li$_{3x}$La$_{2/3-x}$TiO$_3$ exhibits high conductivity [6, 7]. Li$_{3x}$La$_{2/3-x}$TiO$_3$ has attracted much attention due to its potential application in high energy density power source, chemical sensor and ion selective electrode [7, 8, 9, 10]. LLTO has a high grain conductivity of 10^{-3} S cm^{-1} at room temperature. [11, 12] Meanwhile, LLTO is stable against atmosphere. But its total conductivity is still too low to application [13, 14]. In LLTO, Li$^+$ and La^{3+} occupied A-site while Ti^{4+} occupied B-site, Li ions migrate via vacancies in A-sites [14, 15]. Li$^+$ conduction comply with vacancy mechanism that Li ions move through square planar bottleneck between A-sites [16]. So its conductivity is related to vacancy concentration and bottleneck size [17]. High valence elements doping in B-site can increase vacancy concentration of LLTO. Generally B-site in LLTO can tolerate multifarious cations with various radii and valence such as trivalent Al^{3+}, Y^{3+} and pentavalent Nb^{5+}, Ta^{5+} [18, 19, 20]. Hetero-valent elemental doping is an effective way to improve conductivity of perovskite solid electrolytes [21, 22]. The doping of trivalent cations such as Al, Y and Yb at the B site of perovskite results in an increasement for the conductivity of LLTO [20, 21, 22]. Furthermore, covering with mother powder during sintering lead to materials waste. ZrO$_2$ powder is much cheaper than mother powder [23]. Here we also investigated the substitution of ZrO$_2$ powder for mother powder to protect pellets during sintering.

In this work, W-doped Li$_{0.39}$La$_{0.54}$TiO$_3$ perovskite solid electrolyte was prepared by using mother-powder-bed sintering method and ZrO$_2$-powder-bed sintering method, respectively. Influence of sintering method on crystalline structure for W-doped Li$_{0.39}$La$_{0.54}$TiO$_3$ was studied. Effect of Tungsten (W) doping on crystalline structure, microstructure, and conductivity for Li$_{0.39}$La$_{0.54}$TiO$_3$ was investigated.

2. Experimental

W-doped Li$_{0.39}$La$_{0.54}$TiO$_3$ was prepared via conventional solid state reaction. Li$_2$CO$_3$ (98%, Aladdin), La$_2$O$_3$ (99.9%), TiO$_2$ (99%, GUOYAO), WO$_3$ (99.9%, GUOYAO) were weighted in stoichiometric amounts and mixed in ethanol by ball milling and then calcined at 900 °C for 10 h. The obtained powders were reground in agate mortar and pressed into pellets at the pressure of 200 MPa by cold isostatic pressing. Diameter of all ceramic pellets is 15 mm. Finally, W-doped Li$_{0.39}$La$_{0.54}$TiO$_3$ perovskite solid electrolyte pellets were sintered at

1350 °C for 6 h. Sintering steps of W doped LLTO solid electrolytes was shown in Fig. 1.
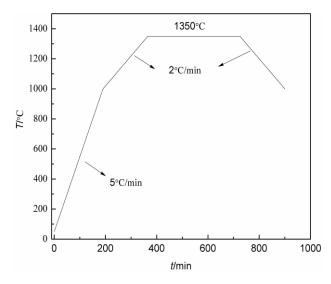

Fig. 1. Sintering steps of W doped LLTO solid electrolytes

Pellets were cover with mother powder or ZrO$_2$ powder during sintering. Crystalline structure of all samples was characterized by X-ray diffraction on X pert PRO (Panalytiacl) using Cu Kα radiation between 5° and 90°. Scanning electron microscope (SEM) was performed using SSX-550 (SHIMADZU). Ionic conductivity of pellets was evaluated by AC-impedance technology on Solartron 1260 at frequency from 1 Hz to 10 MHz in the temperature ranged from 10 °C to 140 °C. Before the measurement of conductivity, both surface of ceramic pellets were polished and pained a layer of Au as electrodes.

3. Results and discussion

Fig. 2 shows X-ray patterns of W-doped LLTO sintered by using mother powder-bed sintering. The main diffraction peaks of W-doped LLTO are corresponding with Li$_{0.35}$La$_{0.55}$TiO$_3$ (PDF#46-0465), indicate that W-doped LLTO has perovskite structure. A small amount of La$_2$Ti$_2$O$_7$ impurity phase was observed in each ceramic pellet. The presence of Li-deficient impurity phase La$_2$Ti$_2$O$_7$ was attributed to the loss of lithium during high temperature sintering.
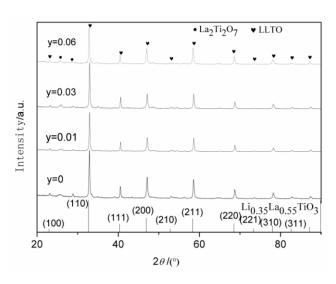

Fig. 2. X-ray patterns of W-doped LLTO sintered by mother-powder-bed method

Fig. 3 shows X-ray patterns of W-doped LLTO pellets sintered by using ZrO$_2$ powder-bed sintering. W-doped LLTO pellets sintered with ZrO$_2$ powder present perovskite structure, which is similar to pellets sintered with mother powder. The peak intensity of Li-deficient La$_2$Ti$_2$O$_7$ impurity phase in W-doped LLTO sintered by ZrO$_2$-powder-bed method is much larger than that sintered with mother powder. This indicates that the loss of lithium element during high temperature sintering and the formation of Li-deficient La$_2$Ti$_2$O$_7$ impurity phase were suppressed significantly by mother-powder-bed method, but not ZrO$_2$-powder-bed method.
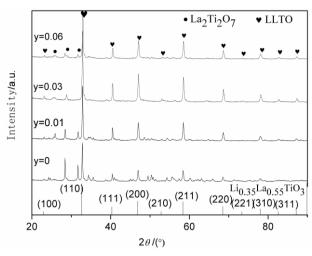

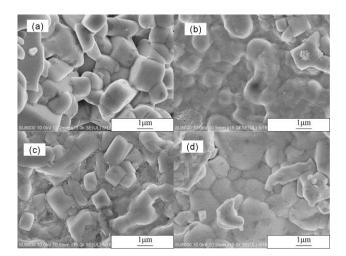*Fig. 3. X-ray patterns of W-doped LLTO sintered by ZrO$_2$-powder-bed method*

Fig. 4. Scanning electron microscope images for W-doped LLTO sintered by mother powder sintering

Fig. 4 shows SEM images of W-doped LLTO sintered by mother powder sintering. As can be seen, grains were well-connected with each other after high temperature sintering at 1350°C for 6 h. But pores also existed in ceramic pellets. This might be attributed to the evaporation of lithium oxide during high temperature sintering and subsequent shrinkage during the growth of grains.
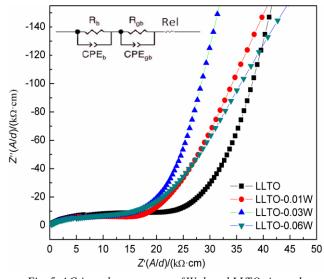

Fig. 5. AC-impedance spectra of W-doped LLTO sintered with mother powder at room temperature (color online)

Fig. 5 shows typical AC-impedance plots for W-doped LLTO sintered by mother powder sintering at room temperature. The shape of this figure corresponds to the typical AC-impedance spectra of fast ionic conducting solid electrolyte. The equivalent circuit $R_{ele}(R_{bulk}Q_{bulk})(R_{gb}Q_{gb})Q$ was used to fit these impedance spectra. Here, R is the resistance and Q is the

constant phase element (CPE). For non-doped LLTO, Li ionnic conductivity is 3.70×10^{-5} S cm^{-1}. This result is in good agreement with previous report. As the content of W dopant increases, conductivity of samples increases first, then decreases. Conductivity of LLTO, LLTO-0.01W, LLTO-0.03W and LLTO-0.06W are 3.70×10^{-5} S cm^{-1}, 0.44×10^{-5} S cm^{-1}, 5.94×10^{-5} S cm^{-1} and 4.40×10^{-5} S cm^{-1}, respectively.
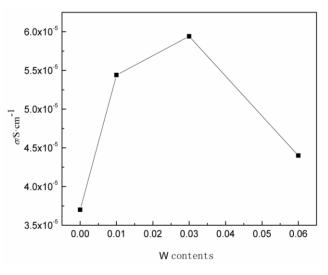

Fig. 6. The W contents dependence of conductivity for W-LLTO

Conductivity of solid electrolytes at room temperature follows this order LLTO-0.03W> LLTO-0.01W> LLTO-0.06W> LLTO. Among these compounds, LLTO-0.03W sample has the highest conductivity of 5.94×10^{-5} S cm^{-1} at room temperature. This result demonstrates that higher conductivity can be obtained for LLTO with hexabasic W doping.
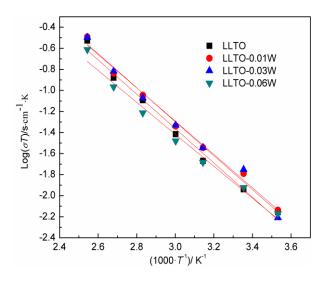

Fig. 7. Arrhenius plots for total conductivity of W-doped LLTO sintered with mother powder (color online)

Fig. 6 shows Arrhenius plots of total conductivity of W-doped LLTO pellets sintered by mother powder sintering. The activation energy was calculated from slope of log (σT) vs. 1000/T plots in the temperature range of 10-140 °C. Activation energy of W-doped LLTO samples was found to be within the range reported for solid state fast Li ion conductors. As the content of W dopant increases, activation energy of samples decreases. Activation energies of LLTO, LLTO-0.01W, LLTO-0.03W and LLTO-0.06W are 0.325 eV, 0.321 eV, 0.314 eV and 0.312 eV, respectively. $Li_{0.3}La_{0.48}Ti_{0.94}W_{0.06}O_3$ presents the lowest activation energy of 0.312.

4. Conclusion

In summary, Tungsten (W) doped perovskite-type $(Li_{0.39}La_{0.54})_{(1-x)}Ti_{(1-x)}W_xO_3$ (x=0, 0.01, 0.03, 0.06) solid electrolyte was successfully synthesized by conventional solid state method. As the content of W dopant increases, conductivity of W-LLTO increases first, then decreases. LLTO-0.03W (x=0.03) has the highest conductivity of 5.94×10^{-5} S cm^{-1} at room temperature, with activation energy of 0.314 eV in the temperature range of 10-140 °C.

Acknowledgements

References

[1] J. M. Tarascon, M. Armand, Nature **414**, 359 (2001).
[2] J. B. Goodenough, Y. Kim, Chem. Mater. **22**, 587 (2010).
[3] K. Takada, Acta Mater. **61**, 759 (2013).
[4] J. C Bachman, S. Muy, A. Grimaud, H. H. Chang, N. Pour, F. Lux, O. Paschos, F. Maglia, S. Lupart, P. Lamp, L. Giordano, S. H. Yang, Chem. Rev. **116**, 140 (2015).
[5] P. Knauth, Solid State Ionics **180**, 911 (2009).
[6] T. Yang, Y. Li, C. K. Chan, J. Power Sources **287**, 164 (2015).
[7] Y. Kong, Y. Li, J. Lu, Ceram. Int. **43**, 5642 (2017).
[8] H. Wang, J. Cheng, L. Zhai, J. Cheng, Solid State. Commun. **142**, 710 (2007).
[9] S. X. Zhao, X. F. Fan, Y. F. Deng, C. W. Nan, Electrochim. Acta **65**, 7 (2012).
[10] C. Bohnke, B. Regrag, F. Le Berre, J. L. Fourquet, N. Randrianantoandro, Solid State Ionics **176**, 73 (2005).
[11] K. Chen, M. Huang, Y. Shen, C. W. Nan, Electrochim. Acta **80,** 133 (2012).
[12] H. Geng, A. Mei, Y. Lin, C. W. Nan, Mat. Sci. Eng. B. **164**, 91 (2009).
[13] K. P. Abhilash, P. C. Selvin, B. Nalini, P. Nithyadharsenic, B. C. Pillaic, Ceram. Int. **39**, 947 (2013).
[14] C. Ma, K. Chen, C. Liang, C. W. Nan, R. Ishikawa, K. Morea, M. Chi, Energ. Environ. Sci. **7**, 1638 (2014).
[15] O. Bohnke, J. Emery, A. Veron, J. L. Fourquet, J.Y. Buzare, P. Florian, D. Massiot, Solid State Ionics **109**, 25 (1998).
[16] C. Sun, J. Liu, Y. Gong, P. D. Wilkinsone, J. Zhang, Nano Energy **33**, 363 (2017).
[17] J. Q. Zheng, Y. F. Li, R. Yang, G. Li, X. K. Ding, Ceram. Int. **43**, 1716 (2017).
[18] Y. Kong, Y. Li, J. Lu, C. B. Hu, J. Mater. Sci.-Mater. El. **28**, 8621 (2017).
[19] K. V. Babu, V. Veeraiah, Mater. Sci.-Pol. **34**, 605 (2016).
[20] S. García-Martín, A. Morata-Orrantía, M. A. Alario-Franco, J. Rodríguez-Carvajal, U. Amador, Chem Eur.-J. **13**, 5607 (2007).
[21] R. Yu, Q. X. Du, B. K. Zou, Z. Y. Wen, C. H. Chen, J. Power Sources **306**, 623 (2016).
[22] L. X. He, H. I. Yoo, Electrochim. Acta **48**, 1357 (2003).
[23] R. Inada, K. Kimura, K. Kusakabe, T. Tojo, Y. Sakurai, Solid State Ionics **261**, 95 (2014).

*Corresponding author: liying@smm.neu.edu.cn